Published in final edited form as:
Astron Astrophys. ; 649: . doi:10.1051/0004-6361/202140978.

O-bearing complex organic molecules at the cyanopolyyne peak of TMC-1: detection of C_2H_3CHO, C_2H_3OH, $HCOOCH_3$, and CH_3OCH_3 ★

M. Agúndez[1], **N. Marcelino**[1], **B. Tercero**[2,3], **C. Cabezas**[1], **P. de Vicente**[3], **J. Cernicharo**[1]

M. Agúndez: marcelino.agundez@csic.es; J. Cernicharo: jose.cernicharo@csic.es

[1]Instituto de Física Fundamental, CSIC, Calle Serrano 123, E-28006 Madrid, Spain

[2]Observatorio Astronómico Nacional, IGN, Calle Alfonso XII 3, E-28014 Madrid, Spain

[3]Observatorio de Yebes, IGN, Cerro de la Palera s/n, E-19141 Yebes, Guadalajara, Spain

Abstract

We report the detection of the oxygen-bearing complex organic molecules propenal (C_2H_3CHO), vinyl alcohol (C_2H_3OH), methyl formate ($HCOOCH_3$), and dimethyl ether (CH_3OCH_3) toward the cyanopolyyne peak of the starless core TMC-1. These molecules are detected through several emission lines in a deep Q-band line survey of TMC-1 carried out with the Yebes 40m telescope. These observations reveal that the cyanopolyyne peak of TMC-1, which is the prototype of cold dark cloud rich in carbon chains, contains also O-bearing complex organic molecules like $HCOOCH_3$ and CH_3OCH_3, which have been previously seen in a handful of cold interstellar clouds. In addition, this is the first secure detection of C_2H_3OH in space and the first time that C_2H_3CHO and C_2H_3OH are detected in a cold environment, adding new pieces in the puzzle of complex organic molecules in cold sources. We derive column densities of $(2.2 \pm 0.3) \times 10^{11}$ cm™2, $(2.5 \pm 0.5) \times 10^{12}$ cm^{-2}, $(1.1 \pm 0.2) \times 10^{12}$ cm^{-2}, and $(2.5 \pm 0.7) \times 10^{12}$ cm^{-2} for C_2H_3CHO, C_2H_3OH, $HCOOCH_3$, and CH_3OCH_3, respectively. Interestingly, C_2H_3OH has an abundance similar to that of its well known isomer acetaldehyde (CH_3CHO), with C_2H_3OH/CH_3CHO ~ 1 at the cyanopolyyne peak. We discuss potential formation routes to these molecules and recognize that further experimental, theoretical, and astronomical studies are needed to elucidate the true mechanism of formation of these O-bearing complex organic molecules in cold interstellar sources.

Keywords

astrochemistry; line: identification; ISM: individual objects (TMC-1); ISM: molecules; radio lines: ISM

★Based on observations carried out with the Yebes 40m telescope (projects 19A003, 20A014, and 20D023). The 40m radiotelescope at Yebes Observatory is operated by the Spanish Geographic Institute (IGN, Ministerio de Transportes, Movilidad y Agenda Urbana).

Europe PMC Funders Author Manuscripts

1 Introduction

Complex organic molecules (COMs) like methyl formate ($HCOOCH_3$) and dimethyl ether (CH_3OCH_3) have been traditionally observed in the warm gas around protostars, the so-called hot cores and corinos, where they are thought to form upon thermal desorption of ice mantles on grains (Herbst & van Dishoeck 2009). In the last decade, these molecules have been observed as well in a few cold sources, like the dense cores B1-b (Öberg et al. 2010; Cernicharo et al. 2012) and L483 (Agúndez et al. 2019), the dark cloud Barnard 5 (Taquet et al. 2017), the pre-stellar cores L1689B (Bacmann et al. 2012) and L1544 (Jiménez-Serra et al. 2016), and the starless core TMC-1 (Soma et al. 2018). The low temperatures in these environments inhibit thermal desorption, and it is still an active subject of debate how are these molecules formed, whether in the gas phase or on grain surfaces followed by some non-thermal desorption process (Vasyunin & Herbst 2013; Ruaud et al. 2015; Balucani et al. 2015; Chang & Herbst 2016; Vasyunin et al. 2017; Shin-gledecker et al. 2018; Jin & Garrod 2020).

The cyanopolyyne peak of TMC-1, TMC-1(CP), is characterized by a carbon-rich chemistry, with high abundances of carbon chains and a poor content of O-bearing COMs (e.g., Agúndez & Wakelam 2013). Here we report the detection of four O-bearing COMs toward TMC-1(CP). Propenal (C_2H_3CHO) has been reported previously toward massive star-forming regions in the Galactic center (Hollis et al. 2004; Requena-Torres et al. 2008) and in the hot corino IRAS 16293-2422B (Manigand et al. 2021). Vinyl alcohol (C_2H_3OH) has been only seen toward Sagittarius B2(N), where the high spectral density complicates the identification (Turner & Apponi 2001). Therefore, this is the first clear detection of C_2H_3OH in space and the first time that C_2H_3CHO and C_2H_3OH are detected in a cold environment. We also report the detection of $HCOOCH_3$ and CH_3OCH_3, recently detected (the latter tentatively) toward the methanol peak of TMC-1 (Soma et al. 2018) but not toward TMC-1(CP).

2 Astronomical observations

The data presented here belong to a Q-band line survey of TMC-1(CP), $\alpha_{J2000} = 4^h41^m41.9^s$ and $\delta_{J2000} = +25°41'27.0''$, performed with the Yebes 40m telescope. The cryogenic receiver for the Q band, built within the Nanocosmos project[1] and which covers the 31.0-50.4 GHz frequency range with horizontal and vertical polarizations, was used connected to FFTS spectrometers, which cover a bandwidth of 8×2.5 GHz in each polarization with a spectral resolution of 38.15 kHz. The system is described in Tercero et al. (2021). The half power beam width (HPBW) of the Yebes 40m telescope ranges from 36.4″ to 54.4″ in the Q band. The intensity scale is antenna temperature, T_A^*, for which we estimate an uncertainty of 10 %, which can be converted to main beam brightness temperature, T_{mb}, by dividing by B_{eff}/F_{eff} (see Table 1). The line survey was carried out during several observing runs and various results have been already published. Data taken during November 2019 and February 2020 allowed to detect the negative ions C_3N^- and C_5N^- (Cernicharo et al. 2020a), and to discover HC_4NC (Cernicharo et al. 2020b), HC_3O^+

[1] https://nanocosmos.iff.csic.es

(Cernicharo et al. 2020c), and HC_5NH^+ (Marcelino et al. 2020). A further observing run, carried out in October 2020, resulted in the detection of HDCCN (Cabezas et al. 2021), HC_3S^+ (Cernicharo et al. 2021a), CH_3CO^+ (Cernicharo et al. 2021b), and various C_4H_3N isomers (Marcelino et al. 2021). Additional observations were taken in December 2020 and January 2021, which led to the discovery of vinyl acetylene (CH_2CHCCH; Cernicharo et al. 2021c), allenyl acetylene ($CH_2CCHCCH$; Cernicharo et al. 2021d), and propargyl (CH_2CCH; Agúndez et al. 2021), and a final run was carried out in March 2021. All observations were carried out using the frequency switching technique, with a frequency throw of 10MHz during the two first observing runs and 8MHz in the later ones. All data were reduced with the program CLASS of GILDAS (Pety 2005)[2].

3 Molecular spectroscopy

C_2H_3CHO has two conformers. The most stable, and the only one reported in space (Hollis et al. 2004; Requena-Torres et al. 2008; Manigand et al. 2021), is the *trans* form, which is the one reported here as well. Level energies and transition frequencies were obtained from the rotational constants derived by Daly et al. (2015). The dipole moment along the *a* axis (all transitions observed here are of a-type) is 3.052D (Blom et al. 1984).

C_2H_3OH has also two conformers, named *syn* and *anti.* Turner & Apponi (2001) assigned various emission features to the two conformers in the crowded spectra of Sgr B2(N). Here we report an unambiguous detection of the *syn* form, which is the most stable one, in a colder source that is much less affected by line confusion. Level energies and transition frequencies were computed from the rotational constants given by Melosso et al. (2019). The components of the dipole moment along the *a* and *b* axes are 0.616 D and 0.807 D, respectively (Saito 1976). Both *a*- and *b*-type transitions are observed here.

$HCOOCH_3$ is a well known interstellar molecule in which the internal rotation, or torsion, of the methyl group makes each rotational level to split into *A* and *E* substates, with statistical weights A:E = 1:1. We used the spectroscopy from a fit to the lines measured by Ogata et al. (2004) implemented in MADEX (Cernicharo et al. 2012). Here all observed transitions are of *a*-type and thus we adopted μ_a = 1.63 D (Curl 1959).

CH_3OCH_3 is an asymmetric rotor in which the large amplitude internal motion of the two equivalent methyl groups leads to level splitting into AA, EE, EA, and *AE* substates, with nontrivial statistical weights (Endres et al. 2009). We adopted the spectroscopy from the CDMS catalog (Müller et al. 2005) [3]. The geometry of the molecule makes it to have non-zero dipole moment only along the *b* axis, with a measured value of 1.302 D (Blukis et al. 1963).

4 Results

We detected various lines for each of the O-bearing COMs target of this study (see Table 1), with signal-to-noise ratios (S/N) well above 3 σ. The position of the lines is consistent with

[2] http://www.iram.fr/IRAMFR/GILDAS
[3] https://cdms.astro.uni-koeln.de/

the calculated frequencies based on laboratory data (see Sec. 3) and the systemic velocity of the source, V_{LSR} = 5.83 km s^{-1} (Cernicharo et al. 2020b). Moreover, the relative intensities of the lines are those expected for rotational temperatures in the range 3-10 K, which are typical of TMC-1 (Gratier et al. 2016), and there are no missing lines. We thus consider that the detection of the four O-bearing COMs in TMC-1 is secure. Hereafter we discuss the particularities of each molecule.

The detection of the *trans* form of C_2H_3CHO is very solid since the six observed lines are detected with S/N between 6.5 σ and 19.4 σ and the V_{LSR} of the lines are fully consistent with the systemic velocity of TMC-1 (see Table 1 and Fig. 1). The rotational temperature (T_{rot}) of C_2H_3CHO is not very precisely determined, 7.5 ± 3.5K from a rotation diagram, but synthetic spectra computed under thermodynamic equilibrium indicate that values in the range 5-10K are consistent with the relative intensities observed. We thus adopted T_{rot} = 7.5 K to compute the synthetic spectra and derive the column density. The arithmetic mean of the observed C_2H_3CHO linewidths, 0.71 km s^{-1}, is adopted when computing the synthetic spectra (see Table 1). We also assumed a circular emission distribution with a diameter θ_s = 80”, as observed for various hydrocarbons in TMC-1 (Fossé et al. 2001). For the other three molecules we followed the same convention, adopting as linewidth the average of the observed values and assuming the same emission distribution. The column density derived for C_2H_3CHO is (2.2 ± 0.3) × 10^{11} cm^{-2}.

In the case of C_2H_3OH (see Table 1 and Fig. 2), three lines are clearly detected, with S/N of 6.7 σ and 9.0 σ. The frequency of the $2_{1,2}$−$1_{1,1}$ transition, 37459.184 MHz, coincides with a hyperfine component of CH_2CCH, recently reported in TMC-1 (Agúndez et al. 2021). We predict T_A^*, = 1.1 mK for the $2_{1,2}$−$1_{1,1}$ transition, which indicates that the observed line (see Agúndez et al. 2021) has contributions from both CH_2CCH and C_2H_3OH. The high detection significance of three lines, the overlap of a fourth line with CH_2CCH, and the fact that there are no missing lines, makes us to consider the detection of C_2H_3OH secure. The rotational temperature is not well constrained for C_2H_3OH, although the observed relative intensities indicate that it must be in the high range of the values typically observed in TMC-1. We thus adopted T_{rot} = 10K and a linewidth of 0.87 km s^{-1} to compute the synthetic spectra. We derive a column density of (2.5 ± 0.5) × 10^{12} cm^{-2} for C_2H_3OH.

We detected five *A*/*E* doublets of $HCOOCH_3$ with S/N in the range 5.8-14.6 σ (see Table 1 and Fig. 3). The only line affected by a problem is the $3_{0,3}$−$2_{0,2}$ transition of the *E* substate, which accidentally lies close to a negative frequency-switching artifact, making it to appear less intense and slightly shifted from the correct position. We thus did not fit this line. The rotational temperature derived is 5.1 ± 2.5 K, and we thus adopted T_{rot} = 5 K, and a linewidth of 0.67 km s^{-1}, to compute the synthetic spectra. The total column density obtained for $HCOOCH_3$, including both *A* and *E* substates, is (1.1 ± 0.2) × 10^{12} cm^{-2}.

For CH_3OCH_3, we observed four triplets with the characteristic structure of an intense component corresponding to the *EE* substate lying between two equally intense components corresponding to the *AE*+*EA* and *AA* substates. The *EE* component of the four triplets is detected with good confidence levels, between 5.0 σ and 9.6 σ (see Table 1 and Fig. 4). The weaker components corresponding to the *AE*+*EA* and *AA* substates are sometimes found to

lie within the noise, although the computed synthetic spectra is consistent with this fact. We consider that the detection of CH_3OCH_3 is secure. From a rotation diagram we derive a low rotational temperature of 3.6 ± 0.6 K, which is well constrained by the availability of transition covering upper level energies from 2.3K to 10.8 K. We thus adopted T_{rot} = 3.6K and a linewidth of 0.72 km s^{-1} to compute the synthetic spectra, which implies a total column density, including the four substates, of (2.5 ± 0.7) × 10^{12} cm^{-2} for CH_3OCH_3.

The variation in the column densities due to the uncertainty in T_{rot} is small, ~ 15 %, for C_2H_3CHO and C_2H_3OH, and higher, a factor of two, for $HCOOCH_3$ and CH_3OCH_3.

5 Discussion

The abundances derived for C_2H_3CHO, C_2H_3OH, $HCOOCH_3$, and CH_3OCH_3 are 2.2 × 10^{-11}, 2.5 × 10^{-10}, 1.1 × 10^{-10}, and 2.5 × 10^{-10}, respectively, relative to H_2, if we adopt a column density of H_2 of 10^{22} cm^{-2} (Cernicharo & Guélin 1987). Now, how are these four O-bearing COMs formed in TMC-1?.

C_2H_3CHO and C_2H_3OH could be formed by gas-phase neutral-neutral reactions between reactive radicals like OH, CH, or C_2H and abundant closed-shell molecules. However, among the potential sources of C_2H_3OH, the reactions OH + C_2H_4 and OH + CH_2CHCH_3 seem to have activation barriers (Zhu et al. 2005; Zádor et al. 2009) and the reaction CH + CH_3OH seems to yield H_2CO and CH_3 as products (Zhang et al. 2002). In the case of C_2H_3CHO, a potential formation reaction is OH + allene, but the main products are H_2CCO + CH_3 (Daranlot et al. 2012). Two more promising routes to C_2H_3CHO are the reactions CH + CH_3CHO, which has been found to produce C_2H_3CHO (Goulay et al. 2012), and C_2H + CH_3OH, which to our knowledge has not been studied experimentally or theoretically.

C_2H_3CHO and C_2H_3OH are not specifically considered in the chemical networks UMIST RATE12 (McElroy et al. 2013) or KIDA uva.kida.2014 (Wakelam et al. 2015), but acetaldehyde (CH_3CHO), which is an isomer of C_2H_3OH, is included. Since it often happens that astrochemical databases do not distinguish between different isomers because information is not available, it is conceivable that some of the reactions that are considered to produce CH_3CHO could also form C_2H_3OH. According to a standard pseudo-time-dependent gas-phase chemical model of a cold dark cloud (e.g., Agúndez & Wakelam 2013), there are two main reactions of formation of CH_3CHO. The first is O + C_2H_5, for which formation of C_2H_3OH does not seem to be an important channel, according to experiments (Slagle et al. 1988) and theory (Jung et al. 2011; Vazart et al. 2020). The second is the dissociative recombination of CH_3CHOH^+ with electrons, in which case experiments show that the CCO backbone is preserved with a branching ratio of 23% (Hamberg et al. 2010), so that it is possible that both CH_3CHO and C_2H_3OH are formed. A different route to CH_3CHO starting from abundant ethanol (C_2H_5OH) has been proposed (Skouteris et al. 2018; Vazart et al. 2020), but in L483, the only cold environment where C_2H_5OH has been detected, its abundance is twice smaller than that of CH_3CHO (Agúndez et al. 2019). The column density of CH_3CHO at TMC-1(CP) is (2.7-3.5) × 10^{12} cm^{-2} (Gratier et al. 2016; Cernicharo et al. 2020c), which implies a C_2H_3OH/CH_3CHO ratio of ~ 1. Therefore, if the two isomers are formed by the same reaction, then the branching ratios should be similar.

The reaction CH_3^+ + H_2CO produces CH_4 + HCO^+ (Smith & Adams 1978), and thus it is unlikely to form C_2H_3OH, as suggested by Turner & Apponi (2001).

Grain-surface processes could also form C_2H_3CHO and C_2H_3OH in TMC-1. Experiments show that C_2H_3OH is formed upon proton irradiation of H_2O/C_2H_2 ices (Hudson & Moore 2003), and electron irradiation of CO/CH_4 and H_2O/CH_4 ices (Abplanalp et al. 2016; Bergantini et al. 2017), while C_2H_3CHO is produced after electron irradiation of CO/C_2H_4 ices (Abplanalp et al. 2015). Non-energetic processing of C_2H_2 ices, in which reactions with H atoms and OH radicals occur on the surface, also produces C_2H_3OH (Chuang et al. 2020). It remains however uncertain whether these experimental setups (e.g., in terms of irradiation fluxes and ice composition) resemble those of cold dark clouds. Abplanalp et al. (2016) made an effort in this sense by incorporating the results of electron irradiation experiments in a chemical model of a cold dark cloud, and found that cosmic rays could drive the formation of C_2H_3OH on grain surfaces. Recently, Shingledecker et al. (2019) proposed that C_2H_3CHO can be efficiently formed on grain surfaces by successive reactions of addition of an H atom to HC_3O. This process would also produce propynal (HCCCHO), which make these authors to propose a chemical connection, and thus a potential correlation, between HCCCHO and C_2H_3CHO. If this mechanism is correct, then C_2H_3CHO would be more likely detected in those sources with intense HCCCHO emission (Loison et al. 2016).

There is no yet consensus on how are $HCOOCH_3$ and CH_3OCH_3 formed in cold sources. Models where the synthesis relies on chemical desorption and gas-phase radiative associations usually require a chemical desorption efficiency as high as 10 % (Vasyunin & Herbst 2013; Balucani et al. 2015; Chang & Herbst 2016), which can be relaxed if Eley-Rideal processes (Ruaud et al. 2015), radiation chemistry (Shingledecker et al. 2018), or nondiffussive grain-surface processes (Jin & Garrod 2020) are considered. These models can account for abundances relative to H_2 around 10^{-10} for $HCOOCH_3$ and/or CH_3OCH_3 under certain assumptions, although they rely on yet poorly constrained chemical and physical processes. Astronomical observations pointed out that $HCOOCH_3$ and CH_3OCH_3 could have a chemical connection with CH_3OH, based on the slight abundance enhancement inferred for these O-bearing COMs at the CH_3OH peak with respect to the dust peak in the pre-stellar core L1544 (Jiménez-Serra et al. 2016). The column densities derived here for $HCOOCH_3$ and CH_3OCH_3 at TMC-1(CP) are similar, within a factor of two, to those reported by Soma et al. (2018) at the CH_3OH peak of TMC-1. A coherent study using the same telescope and a detailed radiative transfer model is needed to see if there is a significant abundance enhancement of $HCOOCH_3$ and CH_3OCH_3 at the CH_3OH peak of TMC-1.

6 Conclusions

We reported the detection of C_2H_3CHO, C_2H_3OH, $HCOOCH_3$, and CH_3OCH_3 toward the cyanopolyyne peak of TMC-1. This region, which is a prototypical cold dark cloud with abundant carbon chains, has been revealed as a new cold source where the O-bearing COMs $HCOOCH_3$ and CH_3OCH_3 are present. In addition, we provide the first evidence of two other O-bearing COMs, C_2H_3CHO and C_2H_3OH, in a cold source, the latter being identified unambiguously for the first time in space here. The abundances relative to H_2 derived are a

Europe PMC Funders Author Manuscripts

few 10^{-11} for C_2H_3CHO and a few 10^{-10} for the three other molecules. Interestingly, C_2H_3OH has a similar abundance to its isomer CH_3CHO, with $C_2H_3OH/CH_3CHO \sim 1$. We discuss potential formation routes to these molecules and conclude that further experimental, theoretical, and astronomical studies are needed to shed light on the origin of these COMs in cold interstellar sources.

Acknowledgements

We acknowledge funding support from Spanish MICIU through grants AYA2016-75066-C2-1-P, PID2019-106110GB-I00, PID2019-106235GB-I00, and PID2019-107115GB-C21 and from the European Research Council (ERC Grant 610256: NANOCOSMOS). M.A. also acknowledges funding support from the Ramón y Cajal programme of Spanish MICIU (grant RyC-2014-16277). We thank the anonymous referee for a constructive report that helped to improve this manuscript.

References

Abplanalp MJ, Borsuk A, Jones BM, Kaiser RI. ApJ. 2015; 814:45.
Abplanalp MJ, Gozem S, Krylov AI, et al. PNAS. 2016; 113 7727 [PubMed: 27382172]
Agúndez M, Wakelam V. Chem Rev. 2013; 113 8710 [PubMed: 24099569]
Agúndez M, Marcelino N, Cernicharo J, et al. A&A. 2019; 625 A147
Agúndez M, Cabezas C, Tercero B, et al. A&A. 2021; 647:L10.
Bacmann A, Taquet V, Faure A, et al. A&A. 2012; 541:L12.
Balucani N, Ceccarelli C, Taquet V. MNRAS. 2015; 449:L16.
Bergantini A, Maksyutenko P, Kaiser RI. ApJ. 2017; 841:96.
Blom CE, Grassi G, Bauder A. J Am Chem Soc. 1984; 106 7427
Blukis U, Kasai PH, Myers RJ. J Chem Phys. 1963; 38 2753
Cabezas C, Endo Y, Roueff E, et al. A&A. 2021; 646:L1.
Cernicharo J, Guélin M. A&A. 1987; 176:299.
Cernicharo, J. In: Stehlé, C; Joblin, C; d'Hendecourt, L, editors. European Conference on Laboratory Astrophysics; 2012. 251
Cernicharo J, Marcelino N, Roueff E, et al. ApJ. 2012; 759:L43.
Cernicharo J, Marcelino N, Pardo JR, et al. A&A. 2020a; 641:L9.
Cernicharo J, Marcelino N, Agúndez M, et al. A&A. 2020b; 642:L8.
Cernicharo J, Marcelino N, Agúndez M, et al. A&A. 2020c; 642:L17.
Cernicharo J, Cabezas C, Endo Y, et al. A&A. 2021a; 646:L3.
Cernicharo J, Cabezas C, Bailleux S, et al. A&A. 2021b; 646:L7.
Cernicharo J, Agúndez M, Cabezas C, et al. A&A. 2021c; 647:L2.
Cernicharo J, Cabezas C, Agúndez M, et al. A&A. 2021d; 647:L3.
Chang Q, Herbst E. ApJ. 2016; 819:145.
Chuang K-J, Fedoseev G, Qasim D, et al. A&A. 2020; 635:A199.
Curl RF. J Chem Phys. 1959; 30 1529
Daly AM, Bermúdez C, Kolesniková L, Alonso JL. ApJS. 2015; 218:30.
Daranlot J, Hickson KM, Loison J-C, et al. J Phys Chem A. 2012; 116 10871 [PubMed: 23126232]
Endres CP, Drouin BJ, Pearson JC, et al. A&A. 2009; 504:635.
Fossé D, Cernicharo J, Gerin M, Cox P. ApJ. 2001; 552:168.
Goulay F, Trevitt AJ, Savee JD, et al. J Phys Chem A. 2012; 116 6091 [PubMed: 22229734]
Gratier P, Majumdar L, Ohishi M, et al. ApJS. 2016; 225:25.
Hamberg M, Zhaunerchyk V, Vigren E, et al. A&A. 2010; 522:A90.
Herbst E, van Dishoeck EF. ARA&A. 2009; 47:427.
Hollis JM, Jewell PR, Lovas FJ, et al. ApJ. 2004; 610:L21.

Hudson RL, Moore MH. ApJ. 2003; 586 L107
Jiménez-Serra I, Vasyunin AI, Caselli P, et al. ApJ. 2016; 830:L6.
Jin M, Garrod RT. ApJS. 2020; 249:26.
Jung S-H, Park Y-P, Kang K-W, et al. Theor Chem Acc. 2011; 129:105.
Loison J-C, Agúndez M, Marcelino N, et al. MNRAS. 2016; 456 4101
Manigand S, Coutens A, Loison J-C, et al. A&A. 2021; 645:A53.
Marcelino N, Agúndez M, Tercero B, et al. A&A. 2020; 643:L6.
Marcelino N, Tercero B, Agúndez M, Cernicharo J. A&A. 2021; 646:L9.
McElroy D, Walsh C, Markwick AJ, et al. A&A. 2013; 550:A36.
Melosso M, McGuire BA, Tamassia F, et al. ACS Earth Space Chem. 2019; 3 1189
Müller HSP, Schlöder F, Stutzki J, Winnewisser G. J Mol Struct. 2005; 742:215.
Öberg KI, Bottinelli S, Jørgensen JK, van Dishoeck EF. ApJ. 2010; 716:825.
Ogata K, Odashima H, Takagi K, Tsunekawa S. J Mol Spectr. 2004; 225:14.
Pety, J. SF2A-2005: Semaine de l'Astrophysique Francaise. Ca-soli, F, , et al., editors. EDP; Les Ulis: 2005. 721
Requena-Torres MA, Martín-Pintado J, Martín S, Morris MR. ApJ. 2008; 672:352.
Ruaud M, Loison J-C, Hickson KM, et al. MNRAS. 2015; 447 4004
Saito S. Chem Phys Lett. 1976; 42:399.
Shingledecker CN, Tennis J, Le Gal R, Herbst E. ApJ. 2018; 861:20.
Shingledecker CN, Álvarez-Barcia S, Korn VH, Kästner J. ApJ. 2019; 878:80.
Skouteris D, Balucani N, Ceccarelli C, et al. ApJ. 2018; 854:135.
Slagle IR, Sarzyński D, Gutman D, et al. J Chem Soc Faraday Trans. 1988; 2:84–491.
Smith D, Adams NG. Chem Phys Lett. 1978; 54:535.
Soma T, Sakai N, Watanabe Y, Yamamoto S. ApJ. 2018; 854:116.
Taquet V, Wirström ES, Charnley SB, et al. A&A. 2017; 607:A20.
Tercero F, López-Pérez JA, Gallego JD, et al. A&A. 2021; 645:A37.
Turner BE, Apponi AJ. ApJ. 2001; 561 L207
Vasyunin AI, Herbst E. ApJ. 2013; 769:34.
Vasyunin AI, Caselli P, Dulieu F, Jiménez-Serra I. ApJ. 2017; 842:33.
Vazart F, Ceccarelli C, Balucani N, et al. MNRAS. 2020; 499 5547
Wakelam V, Loison J-C, Herbst E, et al. ApJS. 2015; 217:20.
Zádor J, Jasper AW, Miller JA. Phys Chem Chem Phys. 2009; 11 11040 [PubMed: 19924340]
Zhang, X-b; Liu, J-J; Li, Z-s; , et al. J Phys Chem A. 2002; 106 3814
Zhu RS, Park J, Lin MC. Chem Phys Lett. 2005; 408:25.

Europe PMC Funders Author Manuscripts

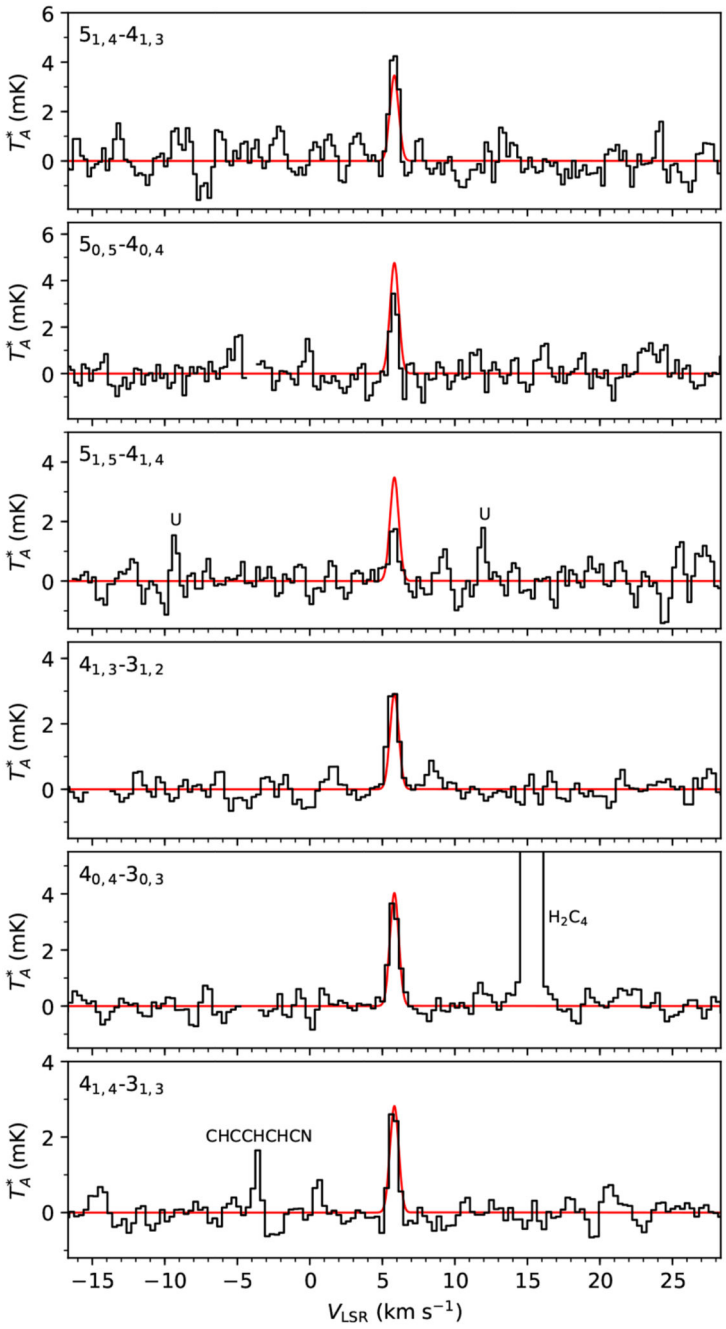

Fig. 1.

Lines of C_2H_3CHO observed in TMC-1 (see parameters in Table 1). In red computed synthetic spectra for $N = 2.2 \times 10^{11}$ cm^{-2}, Trot = 7.5K, FWHM = 0.71 km s^{-1}, and $\theta_s = 80$".

Europe PMC Funders Author Manuscripts

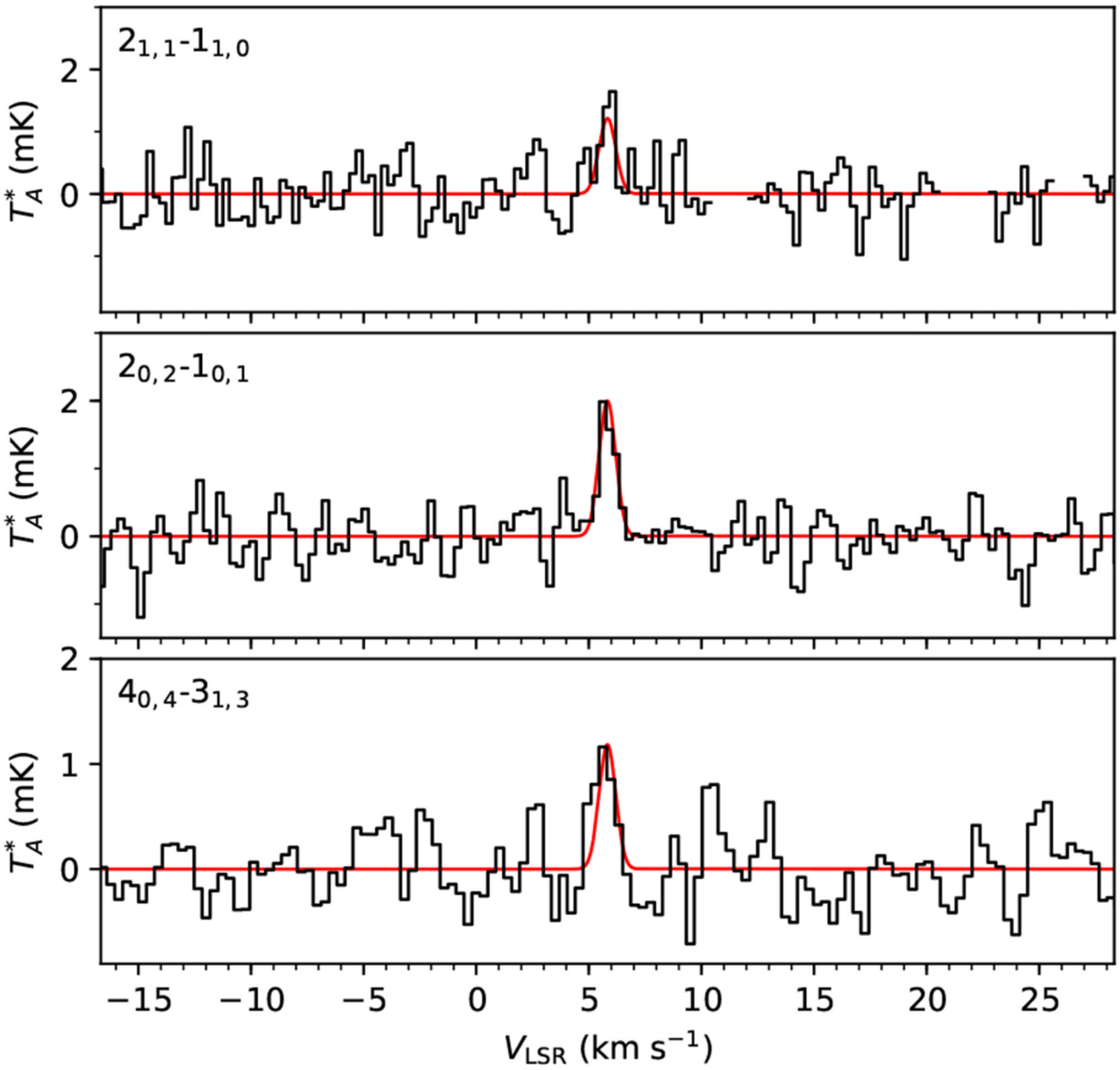

Fig. 2.

Lines of C_2H_3OH observed in TMC-1 (see parameters and note on line $2_{1,1}$–$1_{1,0}$ in Table 1). In red computed synthetic spectra for $N = 2.5 \times 10^{12}$ cm^{-2}, $T_{rot} = 10$ K, FWHM = 0.87 km s^{-1}, and $\theta_s = 80$".

Europe PMC Funders Author Manuscripts

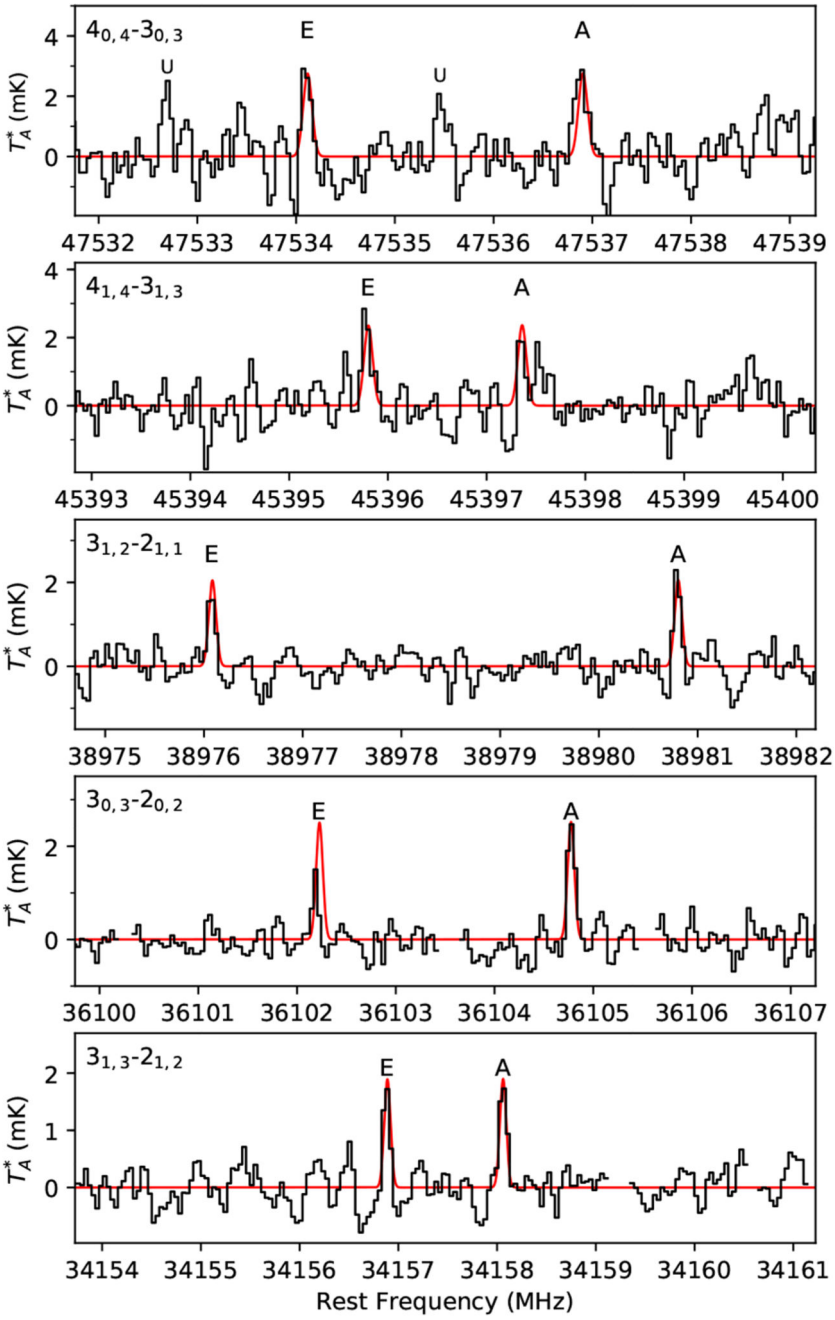

Fig. 3.

Lines of $HCOOCH_3$ observed in TMC-1 (see parameters and note on line $3_{0,3}$-$2_{0,2}$ *E* in Table 1). In red computed synthetic spectra for a $N = 1.1 \times 10^{12}$cm^{-2}, $T_{rot} = 5$ K, FWHM = 0.67 km s^{-1}, and $\theta_s = 80$".

Europe PMC Funders Author Manuscripts

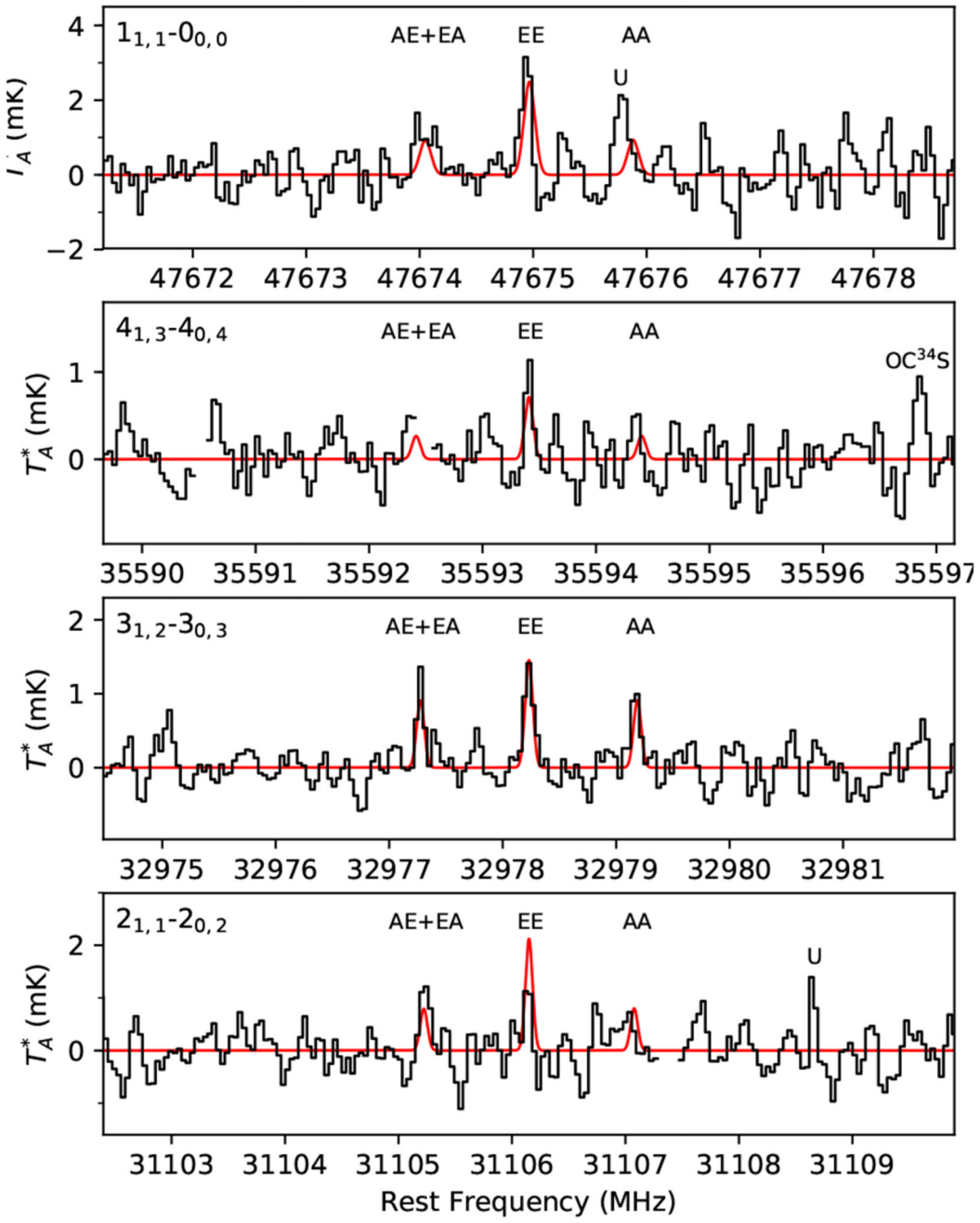

Fig. 4.

Lines of CH_3OCH_3 observed in TMC-1 (see parameters in Table 1). In red computed synthetic spectra for N = 2.5 × 10^{12}cm^{-2}, T_{rot} = 3.6 K, FWHM = 0.72 km s^{-1}, and θ_s = 80".

Table 1

Observed line parameters of the target O-bearing COMs of this study in TMC-1.

Molecule	Transition	E_{up} (K)	ν_{calc} (MHz)	T^*_A peak (mK)	Δv [a] (km s^{-1})	V_{LSR} (km s^{-1})	$\int T^*_A dv$ (mK km s^{-1})	S/N [b] (σ)	B_{eff}/F_{eff} [c]
trans-C_2H_3CHO	$4_{1,4}$-$3_{1,3}$	6.2	34768.987	3.06 ± 0.31	0.62 ± 0.08	5.77 ± 0.03	2.03 ± 0.21	14.5	0.603
	$4_{0,4}$-$3_{0,3}$	4.3	35578.136	3.77 ± 0.33	0.81 ± 0.08	5.79 ± 0.03	3.27 ± 0.27	19.4	0.597
	$4_{1,3}$ −$3_{1,2}$	6.4	36435.990	3.17 ± 0.29	0.85 ± 0.09	5.73 ± 0.04	2.87 ± 0.25	19.2	0.590
	$5_{1,5}$-$4_{1,4}$	8.3	43455.469	1.81 ± 0.49	0.72 ± 0.27	5.78 ± 0.08	1.38 ± 0.37	6.5	0.530
	$5_{0,5}$-$4_{0,4}$	6.4	44449.749	3.67 ± 0.54	0.54 ± 0.08	5.80 ± 0.04	2.11 ± 0.31	10.5	0.521
	$5_{1,4}$-$4_{1,3}$	8.6	45538.994	4.72 ± 0.66	0.69 ± 0.09	5.80 ± 0.04	3.45 ± 0.43	12.6	0.511
syn-C_2H_3OH	$4_{0,4}$-$3_{1,3}$	9.3	32449.221	1.17 ± 0.32	1.07 ± 0.21	5.61 ± 0.11	1.34 ± 0.27	6.8	0.622
	$2_{1,2}$-$1_{1,1}$	5.1	37459.184 [d]	–	–	–	–	–	0.581
	$2_{0,2}$-$1_{0,1}$	2.8	39016.387	1.90 ± 0.39	0.89 ± 0.16	5.81 ± 0.07	1.79 ± 0.29	9.0	0.568
	$2_{1,1}$-$1_{1,0}$	5.3	40650.606	1.71 ± 0.41	0.65 ± 0.19	5.88 ± 0.08	1.18 ± 0.28	6.7	0.554
$HCOOCH_3$	$3_{1,3}$-$2_{1,2}$ *E*	4.0	34156.889	1.92 ± 0.29	0.62 ± 0.12	5.93 ± 0.06	1.27 ± 0.23	9.6	0.608
	$3_{1,3}$-$2_{1,2}$ *A*	3.9	34158.061	1.86 ± 0.29	0.80 ± 0.16	5.84 ± 0.07	1.59 ± 0.28	10.6	0.608
	$3_{0,3}$-$2_{0,2}$ *E*	3.5	36102.227 [e]	–	–	–	–	–	0.593
	$3_{0,3}$-$2_{0,2}$ *A*	3.5	36104.775	2.61 ± 0.29	0.74 ± 0.09	5.80 ± 0.04	2.05 ± 0.22	14.6	0.592
	$3_{1,2}$-$2_{1,1}$ *E*	4.4	38976.085	1.81 ± 0.35	0.66 ± 0.14	5.93 ± 0.07	1.28 ± 0.25	8.3	0.568
	$3_{1,2}$-$2_{1,1}$ *A*	4.4	38980.803	2.45 ± 0.35	0.57 ± 0.09	5.92 ± 0.04	1.49 ± 0.21	10.4	0.568
	$4_{1,4}$-$3_{1,3}$ *E*	6.1	45395.802	2.82 ± 0.57	0.63 ± 0.18	6.00 ± 0.07	1.89 ± 0.40	8.3	0.512
	^{4}1,4-^{3}1,3 A	6.1	45397.360	2.39 ± 0.57	0.42 ± 0.19	5.91 ± 0.10	1.07 ± 0.32	5.8	0.512
	^{4}0,4-^{3}0,3 *E*	5.8	47534.116	3.19 ± 0.75	0.59 ± 0.12	5.92 ± 0.07	2.01 ± 0.44	7.1	0.493
	^{4}0,4-^{3}0,3 *A*	5.8	47536.905	2.76 ± 0.75	0.98 ± 0.23	5.99 ± 0.10	2.88 ± 0.60	7.9	0.493
CH_3OCH_3	$2_{1,1}$ −$2_{0,2}$ *AE* + *EA*	4.2	31105.223	1.35 ± 0.39	0.92 ± 0.25	5.72 ± 0.13	1.31 ± 0.36	5.8	0.632
	$2_{1,1}$-$2_{0,2}$ *EE*	4.2	31106.150	1.52 ± 0.39	0.54 ± 0.34	5.94 ± 0.08	0.87 ± 0.29	5.0	0.632
	$3_{1,2}$-$3_{0,3}$ *AE* + *EA*	7.0	32977.276	1.37 ± 0.25	0.63 ± 0.13	5.84 ± 0.07	0.91 ± 0.19	7.8	0.618
	^{3}1,2-^{3}0,3 *EE*	7.0	32978.232	1.37 ± 0.25	0.95 ± 0.23	5.84 ± 0.09	1.38 ± 0.27	9.6	0.618

Molecule	Transition	E_{up} (K)	ν_{calc} (MHz)	T^*_A peak (mK)	Δv[a] (km s^{-1})	V_{LSR} (km s^{-1})	$\int T^*_A dv$ (mK km s^{-1})	S/N[b] (σ)	B_{eff}/F_{eff}[c]
	$3_{1,2}$-$3_{0,3}$ *AA*	7.0	32979.187	1.06 ± 0.25	0.85 ± 0.32	5.99 ± 0.12	0.96 ± 0.29	7.1	0.618
	$4_{1,3}$-$4_{0,4}$ *EE*	10.8	35593.408	1.22 ± 0.27	0.56 ± 0.13	5.82 ± 0.07	0.73 ± 0.16	6.4	0.597
	$1_{1,1}$-$0_{0,0}$ *EE*	2.3	47674.967	3.31 ± 0.62	0.59 ± 0.12	6.02 ± 0.06	2.08 ± 0.38	8.9	0.492

The line parameters T^*_A peak, Δv, V_{LSR}, and $\int T^*_A dv$ and the associated errors are derived from a Gaussian fit to each line profile.

[a] Δv is the full width at half maximum (FWHM).

[b] Signal-to-noise ratio is computed as S/N = $\int T^*_A dv$ / [rms × $\sqrt{\Delta v \times \delta v (c/\nu_{calc})}$], where c is the speed of light, δv is the spectral resolution (0.03815 MHz), the rms is given in the uncertainty of T^*_A peak, and the rest of parameters are given in the table.

[c] B_{eff} is given by the Ruze formula $B_{eff} = 0.738 \exp[-(\nu/72.2)^2]$, where ν is the frequency in GHz, and $F_{eff} = 0.97$.

[d] Line overlaps with a hyperfine component of CH_2CCH (see Agúndez et al. 2021).

[e] Line detected but not fitted because it overlaps with a negative frequency-switching artifact.